Energy Reports 15 (2026) 109338

Contents lists available at ScienceDirect

Energy Reports

journal homepage: www.elsevier.com/locate/egyr

Research paper

Risk-informed integration of renewable energy systems and storage in electric power grids: Assessing safety and economic viability via an efficient approach

Ozcel Cangul [a], Roberto Rocchetta [b,*], Edoardo Patelli [c]

[a] University of Liverpool, Institute for Risk and Uncertainty, Peach Street, Liverpool, UK
[b] Scuola Universitaria Professionale della Svizzera Italiana, SUPSI-DACD-ISAAC, Intelligent Energy Systems Group, Mendrisio, CH, Switzerland
[c] University of Strathclyde, Department of Civil and Environmental Engineering, James Weir Building, Montrose street, Glasgow, UK

ARTICLE INFO

Keywords:
Energy storage
Photovoltaic
Risk-based optimization
Uncertainty
Power grid
Voltage deviation
Carbon tax analysis

ABSTRACT

Distributed solar and battery storage can lower emissions, cut losses through local self-consumption, and increase autonomy for distribution operators and energy districts. Yet poor siting and sizing, especially under severe weather and random failures, can degrade voltage quality and threaten stability. To achieve low-risk grids and support sustainability goals, enhanced stochastic risk-informed renewable allocation strategies are necessary; not only to quantify and reduce natural uncertainties in the investment, but also to mitigate technical instability risks due to renewable-induced large voltage deviations. To address this challenge, this work introduces a tractable three-stage risk-informed planning framework that: (i) embeds an alternating-current optimal power-flow model inside an event-driven risk assessment procedure; (ii) uses a stratified Monte Carlo scenario generator that includes extreme heatwave events and their impact on electricity demand for cooling; (iii) jointly optimizes a tail-risk measure of voltage deviations (conditional value at risk) together with investment cost; and (iv) links uncertainty drivers to design choices through targeted sensitivity analysis. A carbon-price assessment further quantifies the policy levels required for economic feasibility. A sensitivity analysis is carried out to identify relationships between uncertain parameters and the investment strategy. Applied to the 35-bus North Cyprus system, it delivers two investment plans that balance voltage-risk reduction and cost, and reveals that, even without direct operating-cost savings, battery storage enables higher solar penetration and markedly improves voltage-risk profiles.

1. Introduction

Large-scale investment in distributed generation (DG) and renewable energy sources (RES) is increasingly central to meeting growing electricity demand and sustainability objectives. In particular, photovoltaic (PV) systems coupled with battery energy storage (ES) can reduce CO_2 emissions and transmission losses via local self-consumption (Prakash and Khatod, 2016). Energy storage plays a critical role in mitigating RES variability and improving voltage quality when coordinated intelligently with PV and demand response. Conversely, improper siting, sizing, or inflexible operation of DG/ES can exacerbate voltage deviations and long-term stability risks (R. Li et al., 2020; Munkhchuluun et al., 2020). Robust investment strategies are therefore required to improve voltage profiles (Erdiwansyah et al., 2021) while avoiding severe instabilities and outages (Hadidian-Moghaddam et al., 2018; Munkhchuluun et al., 2020).

Recent large-scale blackouts, such as the Spanish 2025 event (ENTSO-E, 2025), have highlighted modern grid fragility and the need for risk-informed methods. That event caused a near-total outage in Spain and Portugal, disrupting land transportation and communications across multiple states. Vegetation-related faults and voltage-collapse dynamics have been identified as likely contributors (ENTSO-E, 2025). In the literature, extreme weather events (Rocchetta et al., 2018), unforeseen operational scenarios (Zio and Aven, 2011; Nazir and Bollen, 2024), and dynamic instabilities (Garcia-Sanz et al., 2025) are also recognized as significant hazards that can further aggravate the grid risk exposure. In response, European Network of Transmission System Operators for Electricity (ENTSO-E) and Transmission System Operators (TSOs) are complementing traditional $N-1$ security-constrained contingency analysis with *Probabilistic Risk Assessment* (PRA) to capture low-probability, high-impact conditions in operational security limits

* Corresponding author.
E-mail address: roberto.rocchettai@supsi.ch (R. Rocchetta).

https://doi.org/10.1016/j.egyr.2026.109338
Received 10 December 2025; Received in revised form 16 February 2026; Accepted 11 April 2026
Available online 28 April 2026
2352-4847/© 2026 The Authors. Published by Elsevier Ltd. This is an open access article under the CC BY license (http://creativecommons.org/licenses/by/4.0/).

and planning studies. ENSO-E's biennial PRA report clearly documents the shift toward probabilistic coordinated security assessment and risk management across Europe (ENTSO-E, 2023). Parallel research streams include online/proxy-supported PRA for operations (Popli et al., 2024), risk-aware scheduling (Liu et al., 2025), and expansion planning under uncertainty (Tillmanns et al., 2026; Shi et al., 2024; Rahim et al., 2024).

Renewable energy production is inherently uncertain due to variable weather conditions and uncertain dispatch of the generated power. Hence, investments in PV and ES require careful assessment of the associated risks and uncertainties in the long run. Several studies have reviewed methods for mitigating the technical impacts of RES integration (Kow et al., 2016; Huiling et al., 2021; J. Li et al., 2025) and analyzed environmental–operational uncertainties (Monteiro et al., 2020). Both financial and technical aspects are typically considered in planning frameworks (Wong et al., 2019), and the sizing and placement of DG/RES units have been widely studied using different optimization methods and techno-economic indicators (Injeti and Thunuguntla, 2020; Ehsan and Yang, 2018; Javadi et al., 2022; Prasad et al., 2025). In general, the coordinated integration of off-grid PVs (dedicated to charging energy storage) and ES can increase the efficacy of DGs (J. Li et al., 2020), reduce peak demand (Lim et al., 2020; Inaolaji et al., 2024), improve maximum peak load (Mukhopadhyay and Das, 2020), and enable higher penetration of RESs (Rinaldi et al., 2020). However, higher penetration levels also demand supportive energy policies and regulatory instruments, such as carbon taxes, that strongly influence investment feasibility (Zhang et al., 2017; Aldy and Stavins, 2012).

Related works: sizing and siting under extreme weather and voltage tail risks

Risk-aware *Sizing and Siting* (SS) of DG and storage has long combined simulation with multi-objective optimization to account for tail events, e.g., using CVaR to penalize severe voltage deviations (Mena et al., 2014). Complementary studies co-optimize risk and cost for DG under extreme weather, highlighting PRA's role beyond deterministic OPF checks (Rocchetta et al., 2015).Long-term extreme-weather risk received increased attention in planning studies, e.g., in cooperative multi-size transmission expansion (Akdemir et al., 2025) and resilient sizing of battery and hydrogen storage (Ye et al., 2025) under extreme heatwave events. While weather-induced uncertainty has been embedded in infrastructure planning (Khorramfar et al., 2025) and virtual power plant capacity evaluation (C. Li et al., 2025), these studies mainly address bulk systems or capacity adequacy rather than transmission-level voltage-quality risk metrics.

Recent formulations control voltage-security risk via CVaR-averse OPF at the distribution level and learning-assisted risk control with PV, ES, and electric vehicles portfolios (Wang and Song, 2023; Huiling et al., 2021). CVaR-based formulations have been used to manage voltage-deviation risk and optimization, e.g., Lin et al. (2022), albeit primarily focusing on operational and control-oriented rather than long-run planning and event-driven weather effects. On planning, two-stage ESS siting/sizing with demand response and robust ESS allocation address parametric uncertainty but rarely target voltage tail risk directly (Javadi et al., 2022; Peng et al., 2022). For unbalanced distribution systems, a multi-objective Battery Energy Storage Systems (BESS) SS under uncertainty has been proposed in Carpinelli et al. (2024), underscoring the need to manage operational risk explicitly in realistic network models. Broader expansion-planning and operational-risk reviews advocate PRA workflows that retain AC physics while keeping scenarios tractable (Moradi-Sepahvand et al., 2023; Nazir and Bollen, 2024). Recent advances include CVaR-based resilience planning against storms (Bahrami et al., 2023), risk-averse bi-level planning to expand renewable hosting capacity (Zhou et al., 2024), survey frameworks for DGs sizing and siting (Qi et al., 2024), Monte Carlo (MC), augmented placement and hosting-capacity analyses (Iqbal et al., 2025), and safety-aware investment under wildfire risk (Piansky et al., 2025). Large-scale optimization problems have been solved with reduced computational effort while retaining good optimality guarantees, e.g., via decomposition methods (Mei et al., 2016; Liu et al., 2023). Multistage stochastic programming approaches and two-stage SS paradigms have been explored in Javadi et al. (2022). A primary-dual robust reformulation energy storage flexibility problem has been investigated in Wang et al. (2022).

Gaps and contribution of this work

Despite this progress, important gaps remain, particularly concerning:

- (i) **Weather-dependent tail risk in planning:** The risk of non-uniform (weather-dependent) production of decentralized PV units across different geographical areas (Bawazir and Cetin, 2020), over the long run, and exposed to extremes (Cadini et al., 2017; Panteli et al., 2017).
- (ii) **Voltage tail-risk optimization:** Risk due to voltage-related instabilities, particularly *tail risk*, that are rarely assessed explicitly in sizing and siting planning, even though per-unit (p.u.) voltage deviations $|V_i - 1|$ drive quality-of-service concerns;
- (iii) **Scalability with uncertainty:** Scalability to larger networks remains challenging, particularly when incorporating uncertainty, policies, and regulations within the optimization framework (Jain et al., 2017).

These limitations persist in recent coordinated expansion studies (Moradi-Sepahvand et al., 2023), decomposition approaches for large-scale optimization problems (Rodríguez et al., 2021; Piansky et al., 2025), and new tools for operational risk analyses and planning for TSOs (Nazir and Bollen, 2024; Rocchetta et al., 2025).

To address these challenges, this work presents a risk-aware planning workflow that quantifies uncertainty and evaluates a tail-sensitive reliability metric, the CVaR CVaR_α of absolute bus-voltage deviations, within an AC-OPF-in-the-loop simulator. This approach decomposes allocation into three tractable sub-tasks by combining a genetic algorithm, risk-based sizer, and nonlinear programming for ES allocation. Uncertainty due to seasonally varying irradiance and PV production, power demand, component outages, and extreme weather events (heatwaves) is propagated via an efficient Monte Carlo strategy. In contrast to recent heatwave-resilience works (Akdemir et al., 2025; Ye et al., 2025) and CVaR-based control studies (Lin et al., 2022), our workflow explicitly couples heatwave-driven demand inflation with voltage-quality tail optimization in a long-horizon planning context. To improve efficiency and stability, stratified quasi-MC with event-driven triggers and fixed random numbers is proposed. Finally, we include a lifetime economic assessment that maps carbon-price trajectories to discounted net present value (NPV) to indicate policy thresholds for investment feasibility. The main contributions of this work are summarized as follows:

1. We evaluate CVaR_α of large voltage deviation as a planning objective alongside cost, targeting rare high-consequence voltage deviation events.
2. We couple MC scenario evaluation and AC-OPF within a multi-objective search, using stratified quasi-MC and common random numbers to reduce variance and computational burden (Cervan et al., 2023).
3. We implement a three-step allocation (PV siting/sizing, ES siting/sizing, operational dispatch) that preserves physical fidelity while improving scalability on meshed networks.
4. We quantify discounted NPV and infer break-even carbon-price levels for candidate portfolios, linking technical risk to policy-relevant feasibility.

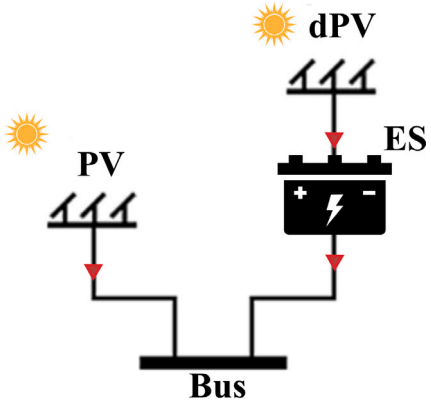


Fig. 1. The proposed operation principle where grid-connected PV and energy storage feed the grid whilst dedicated PV (**dPV**) are for ES charging only.

The remainder of this paper is organized as follows. Section 2 introduces the problem statement and background. Section 3 presents the proposed three-stage risk-informed siting and sizing framework with uncertainty modeling. Section 4 describes the setup for the North Cyprus power grid and reports the results, including risk–cost trade-offs, sampling ablations, and carbon-price sensitivity. Section 5 discusses limitations and implications, and Section 6 concludes this paper.

2. Problem statement

The objective of a siting and sizing problem is to determine an optimal DG allocation tuple that maximizes investment performance in terms of economic return and power quality. The challenge lies in the high dimensionality of real-world grids and the need for long-term, simulation-based analyses that capture both operational dynamics and environmental impacts over the system's lifetime.

2.1. Decision variables

Consider a long-run investment in distributed generators, summarized by the allocation tuple:

$$\mathbf{DG} = \left(\mathbf{PV}, \mathbf{dPV}, \mathbf{ES}^{p}, \mathbf{ES}^{e}\right), \tag{1}$$

with $\mathbf{PV} \in \mathbb{R}_{+}^{n_b}$ denoting grid-connected PV (capacities per bus) injecting power into the grid, $\mathbf{ES}^{p} \in \mathbb{R}_{+}^{n_b}$ the storage power ratings (MW), $\mathbf{ES}^{e} \in \mathbb{R}_{+}^{n_b}$ the storage energy capacities (MWh), and $\mathbf{dPV} \in \mathbb{R}_{+}^{n_b}$ the capacities of *dedicated* off-grid PV units that only charge storage (no direct injection to the grid). In our baseline operation, PV can inject active power to the grid, while **dPV** contributes to the storage state of charge but does not feed loads or the grid directly.

Fig. 1 illustrates this operating principle for one bus. This configuration distinguishes between grid-connected PV, which affects network injections and AC-OPF feasibility, and dedicated PV, which only charges storage and is therefore a planning lever to increase storage energy adequacy without necessarily increasing grid-facing PV injections at constrained nodes. Related PV-storage planning studies highlight that storage sizing/operation can be optimized to meet distinct grid objectives, e.g., voltage support and flexibility, and need not be tied one-to-one to grid injections, see for instance, Nazaripouya et al. (2015) and Gupta and Sossan (2023).

2.2. Deterministic DG allocation

Given an investment horizon with N_t operating time steps, e.g., hourly over one year, and a trajectory for the operational-environmental variables $\{\zeta_t\}_{t=1}^{N_t}$, a deterministic siting and sizing problem seeks an allocation **DG** that minimizes costs while respecting an investment budget B as follows:

$$\min_{\mathbf{DG}} \sum_{t=1}^{N_t} f\left(x_t^{\star}, \zeta_t; \mathbf{DG}\right) \quad \text{s.t.} \quad f_{\text{inv}}(\mathbf{DG}) \le B, \tag{2}$$

where $f_{\text{inv}}(\mathbf{DG})$ is the investment cost, $x_t^{\star} = (\Theta, V, p_g, q_g)_t^{\star}$ is the *optimal operating point*, i.e., voltage phases Θ and magnitudes V in all busses, active/reactive dispatch p_g, q_g for all generators, that minimizes the instantaneous operating grid cost for the chosen **DG** and scenario ζ_t. The operating cost is separated into the cost of fuel for traditional generators and operations and maintenance (O&M) costs as follows:

$$f(x, \zeta; \mathbf{DG}) = f_{\text{fuel}}(x, \zeta; \mathbf{DG}) + f_{\text{O\&M}}(x, \zeta; \mathbf{DG}), \tag{3}$$

with $f_{\text{fuel}}(x) = \sum_{i=1}^{n_b} c_{g,i}\left(p_{g,i}, q_{g,i}\right)$, where $c_{g,i}(\cdot)$ is the marginal fuel costs for the traditional generator at bus i, which depend on ζ and **DG** through the AC-OPF solution $x_t^{\star}$. The O&M costs function $f_{O\&M}$ captures operations and maintenance costs for both traditional generators and DGs. Note that computing $x_t^{\star}$ requires solving a nonconvex AC optimal power flow that accounts for DG injections, as detailed in Mena et al. (2014) and Rocchetta et al. (2015) and outlined in the next section. Accordingly, in this model, the main channel for annual savings in running costs is the reduction of conventional fuel-based generation; curtailment penalties and market revenues for storage are not considered here to reduce complexity.

2.3. AC optimal power flow model

The work adopts a modified Alternating Current Optimal Power Flow (AC-OPF) model to estimate the optimal operating cost as follows Zimmerman et al. (2009). The goal is to find a state x that minimizes the operational costs for the grid:

$$\min_{x} f(x, \zeta; \mathbf{DG}) \tag{4}$$

subject to:

$$\begin{aligned} &g(x, \zeta; \mathbf{DG}) = 0, \quad \text{(AC nodal power balance)} \\ &h(x, \zeta; \mathbf{DG}) \le 0 \quad \text{(Operating limits)}, \end{aligned} \tag{5}$$

where $f(x^{\star}, \zeta; \mathbf{DG})$ is the optimal operating cost from (4), $g(\cdot) = 0$ enforces nodal complex-power balances, and $h(\cdot) \le 0$ collects voltage–magnitude bounds, line/transformer thermal limits, and generator capability constraints. In the balances, net active demand p is offset by grid-connected PV injections p_{pv} and storage dispatch p_{es}. PV and ES are assumed unity power factor (no reactive injection). For clarity, smart-inverter Volt/VAR and curtailment controls (e.g., Zhang et al., 2025; Xiong et al., 2023) are not modeled, although they can materially affect voltage risk and could be incorporated in future work. The injections p_{pv} and p_{es} depend on installed capacities and weather ζ; dedicated off-grid PV affects storage via the state of charge. The presence of DG shifts system reactive requirements, so conventional units adjust q_g to maintain stability; optimization of DG power factor or curtailment is outside the scope of this work.

2.4. Modeling uncertainty

The variables ζ_t represent uncertain environmental–operational states that include both normal and extreme seasonal weather conditions, active and reactive nodal power demands, and unexpected outages at time t. Specifically we define the vector ζ_t at time t as in Cangul (2021). The random vector $\zeta_t := (\omega_t, d_t, a_t)$, comprises weather variables ω_t, i.e., irradiance, cloud cover, heatwaves indicators, with seasonality and spatial heterogeneity; $d_t = (p_d, q_d)_t$ are bus-level active and reactive demands; and a_t are component availability indices (outages) and duration. The variables in ζ_t drives both injections and constraints PV output $p_{pv,i}(t)$ and feasible storage

dispatch $p_{es,i}(t)$ depend on ω_t and the chosen **DG**; nodal balances, voltage limits, and line flows depend on (d_t, a_t). It is not assume independence across buses or time, and the scenario generation model, see Sections 2.5 and 3.1, creates a spatio–temporal correlations and tail behavior (extremes) when generating a data set of trajectories $\left\{\{\zeta_t^{(s)}\}_{t=1}^{N_t}\right\}_{s=1}^{N_s}$. These scenarios are then evaluated via AC-OPF to obtain $x_{t,s}^{\star}$ and the corresponding costs and voltage-risk metrics. Heat-wave indicators are used here to model demand inflation due to cooling load, while PV output is driven by irradiance and cloud cover. Note that temperature-dependent PV efficiency is not explicitly considered here. A scenario generation procedure is adopted from Cangul (2021) and Cangul et al. (2023) to generate representative uncertain scenarios.

2.5. Scenario generation

The hierarchical scenario-generation approach described in Cangul et al. (2023) is adopted in this work and briefly summarized here for completeness and reproducibility. A set of full-year trajectories is generated at hourly resolution. Then, a number n_{mc} of time instants are sampled uniformly from the set and evaluated via AC-OPF to compute voltage- and cost-related metrics.

- **Nodal demand** d_t: Bus-level demand is modeled as a truncated Gaussian random process. At each hour t, the demand state is sampled as $p_{g,i,t} \sim \mathcal{N}(\mu_{i,t}^{p}, \sigma_{i,t}^{p,2})$ and $q_{g,i,t} \sim \mathcal{N}(\mu_{i,t}^{q}, \sigma_{i,t}^{q,2})$ truncated at $\pm 3\sigma_t$. Here $\mu_{i,t}$ represents the mean of the active and reactive power demand at bus i and time t and follows a two-peak daily profile with seasonal modulation as in Cangul et al. (2023) (see Fig. 4), whilst standard deviation is determined assuming a coefficient of variation 5% representing the stochastic variability.
- **Weather scenarios** ω_t: *Irradiance and cloud cover:* Hourly irradiance is modeled as a non-stationary Gaussian process with hour-dependent mean and variance estimated from historical data, truncated to enforce physical bounds (non-negative irradiance). The net irradiance is obtained from the clear-sky component modulated by stochastic cloud coverage, following Cangul et al. (2023) (see Fig. 5) and data from measurements measured in Kalkanli, Cyprus (Department of Meteorology and Republic of Cyprus, 2022). *Heat waves:* Heat-wave events are modeled at daily resolution as in Cangul et al. (2023). The number of heat-wave days is sampled from a non-homogeneous Poisson process with rate $\lambda_E > 0$ during in July–August and negligible otherwise.
- **Outages** a_t: Component malfunctions are modeled via Poisson occurrence processes and stochastic durations. For each component i, outage occurrences over the year are sampled from a homogeneous Poisson process with expected number of events λ_i per year; outage durations are sampled from $\mathcal{N}(\mu_{\tau,i}, \sigma_{\tau,i})$, i.e., a truncated normal distribution with parameters $\mu_{\tau,i}$ and deviation $\sigma_{\tau,i}$ for component i. The sampled event times and durations are mapped into the component availability indicators a_t used by the AC-OPF at each evaluated instant.

2.6. Stochastic DG allocation

Problem (2) is deterministic because a single trajectory $\{\zeta_t\}_{t=1}^{N_t}$ is accounted for. When realized conditions differ, the optimized DG SS plan can underperform. A risk-aware alternative replaces the single trajectory with a *tail-sensitive* objective on operating cost using Conditional Value-at-Risk (CVaR):

$$0 \min_{\mathbf{DG}} \sum_{t=1}^{N_t} \mathrm{CVaR}_{\alpha}\big(f\big) \quad \text{s.t.} \quad f_{\mathrm{inv}}(\mathbf{DG}) \le B, \tag{6}$$

where $\alpha \in\in [0, 1)$ is a probability level and controls the risk aversion. Note that for $\alpha = 0$, the objective coincides with the *expected* cost and risk-neutral planning, i.e., $\mathrm{CVaR}_0(f) = \mathbb{E}_{\zeta_t}(f)$. On the other hand, $\alpha \to 1$, CVaR_{α} approaches a *worst-case* robust formulation, yielding a conservative min–max-like design. Intermediate values of α lead to different risk aversion levels in terms of uncertainty in the financial objective $f\big(x_t^{\star}, \zeta_t; \mathbf{DG}\big)$. In practice, (6) can be solved via a sample-average approximation with N_s scenarios per time step using the Rockafellar–Uryasev auxiliary form (Rockafellar et al., 2000). Let $x_{t,s}^{\star}$ denote the AC-OPF solution for scenario $\zeta_t^{(s)}$. The program is given as follows:

$$\min_{\mathbf{DG}, \eta_t, u_t \ge 0} \sum_{t=1}^{N_t} \left[\eta_t + \frac{1}{(1-\alpha)\, N_s} \sum_{s=1}^{N_s} u_t^{(s)} \right] \tag{7}$$

subject to:

$$u_t^{(s)} \ge f\big(x_t^{\star(s)}, \zeta_t^{(s)}; \mathbf{DG}\big) - \eta_t, \quad \forall t, s, \tag{8}$$

together with the budget constraint and the operational AC-OPF sub-problems that define $x_t^{\star(s)}$. Formulation (7) controls the financial tail of operating cost; however, technical risks, stability/voltage, are neglected. In Section 3 we will introduce a technical tail metric, $\mathrm{CVaR}_{\alpha}(V)$ to study technical risks. Computational challenges remain due to large n_b, N_t, N_s, and high-dimensional ζ_t and Section 3 introduces a decomposed workflow to address these tractability issues.

3. Decomposition approach for optimal sizing and siting

An optimization procedure is proposed for the allocation of the three technological solutions as shown in Fig. 1, i.e., directly connected PV, dedicated PV, and Energy Storage units, that define the vector **DG**. The sizing and siting of these technologies, addressed through a monolithic approach like the one in the optimization program (7), is hardly tractable for large and complex power grids. To overcome this issue, the stochastic global optimization is addressed via a three-stage heuristic search, which decomposes the sizing and siting problem into three manageable sub-tasks. This is consistent with modern decomposition for stochastic programs, e.g., Mei et al. (2016), Liu et al. (2023) and Wang et al. (2022). The proposed procedure is the following:

> **Stage I** — Risk-based optimization of PV that minimizes an indicator of the risk of large voltage deviations.
> **Stage II** — Risk–cost optimization of ES to minimize both the risk of large voltage deviations and investment costs using a bi-objective optimization.
> **Stage III** — Optimal investment on dedicated PV to maximize an availability index on the energy stored in the energy storage units.

Fig. 2 presents the proposed three-stage heuristic workflow for siting and sizing PV, energy storage, and dedicated PV. For each stage, the figure summarizes the optimizer/solver employed, the objectives minimized, and the corresponding outputs passed to subsequent stages.

3.1. Uncertainty quantification and risk of large voltage deviations

A realistic risk–cost assessment requires propagating operating uncertainty through the grid model and quantifying the tail behavior of voltage quality. A modified MC simulation procedure is developed to estimate the distribution of voltage deviations at each bus, denoted as $F_{|V_i-1|}$, and calculate the overall grid's risk of experiencing significant voltage deviations. The Conditional Value-at-Risk (Rockafellar et al., 2000), denoted by $CVaR_{\alpha}$, is used as a metric to quantify the risk of large unwarranted voltage deviations. The risk is calculated by computing the probabilities of the events that produce large voltage deviation and their associated magnitudes/severity. A detailed definition of the CVaR for large voltage deviations is given in Appendix A. For the characterization of the distribution $F_{|V_i-1|}$, the uncertainty model proposed in Cangul (2021) and Cangul et al. (2023) is exploited. The uncertainty model accounts for various factors such as stochastic power

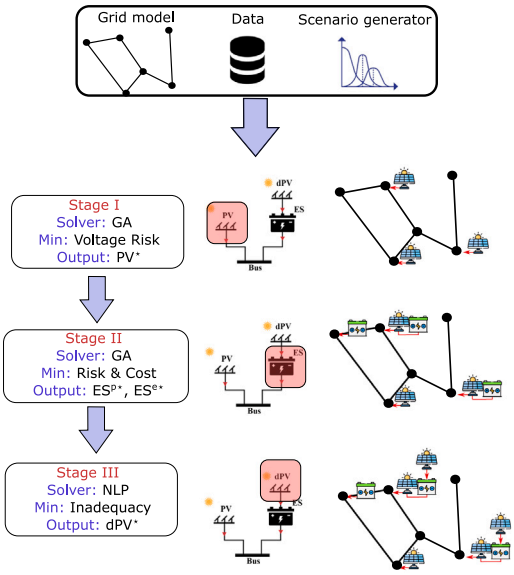


Fig. 2. Three-stage heuristic workflow. **Stage I**: grid-connected PV siting/sizing via voltage-deviation tail-risk minimization. **Stage II**: storage power allocation via a bi-objective trade-off between voltage-risk reduction and investment cost. **Stage III**: dedicated PV sizing for ES charging.

demand, random cloud coverage affecting irradiance and PV production, component failures like line outages and generator shutdowns. The reader is reminded to Cangul et al. (2023) for a more detailed description. Fig. 3 illustrates the proposed MC simulator. A numerical convergence analysis is carried out and discussed in the case study (see Section 4 and Fig. 5). The main steps of the MC simulator are summarized as follows:

- **Generate Scenarios** (Blue Boxes): Similarly to Cervan et al. (2023), this work uses stratified MC draws with event triggers, e.g., heat waves, high-PV, low-load, to reduce estimator variance and facilitate convergence of the stochastic optimization models. Scenario generation follows the hierarchical, event-triggered (stratified) Monte Carlo procedure described in Cangul et al. (2023). For completeness and reproducibility, the sampling mechanism and all probabilistic parameters used in this study are summarized in Section 2.5.
- **Grid Performance Evaluation** (Red Boxes): For each scenario, the AC-OPF is solved and a post-contingency $N-1$ feasibility check carried out on the k most critical lines (with re-dispatch), as in Morsy et al. (2022). The voltage deviation $|V_i - 1|$ in p.u. is computed for each bus, together with fuel and network operational costs.
- **Output Post-Processing** (Green Boxes): Compute the statistical indicators of performance, i.e., the risk of large voltage deviation $CVaR_\alpha$ (see Appendix A) and total network costs. This is consistent with CVaR-averse OPF formulations, e.g., Wang and Song (2023) and Huiling et al. (2021).

3.2. The 3-stages optimization procedure

Due to the large design space and the probabilistic, nonconvex nature of the risk metric (Rocchetta and Crespo, 2021), gradient-based methods are unsuitable for Stages I–II. Accordingly, stochastic evolutionary optimizers (e.g., genetic algorithms) are employed for the PV risk-only sizing and the ES risk–cost sizing, consistent with prior voltage-profile optimizations via evolutionary search (Peng et al., 2022). In Stage III (dedicated PV sizing), a nonlinear programming solver is used: each bus is treated independently with a single design variable, and one NLP is solved per ES-equipped node. Objective functions and solvers thus differ across PV, ES, and dedicated-PV stages as detailed below.

Stage I: Risk-based optimization of PV generators

This stage selects grid-connected PV capacities per bus by minimizing a tail-sensitive voltage-risk metric. Let $\mathbf{PV} \in \mathbb{R}_+^{n_b}$ and $PV_T := \sum_{i=1}^{n_b} PV_i$. The problem is

$$\mathbf{PV}^\star = \arg\min_{\mathbf{PV}\in\mathbb{R}_+^{n_b}} J_I(\mathbf{PV}) \tag{9}$$

subject to

$$0 \le PV_i \le \bar{b}^{PV} \quad \forall i, \qquad 0 \le PV_T \le \bar{b}^{T_{PV}}, \tag{10}$$

where the objective function $J_I(\mathbf{PV}) = \mathrm{CVaR}_\alpha(V;\mathbf{PV})$ is the system-level conditional value-at-risk of per-unit voltage deviations at level α, whilst $\bar{b}^{PV}$ and $\bar{b}^{T_{PV}}$ are the per-bus capacity bounds and the system-wide cap capacity, respectivelly. The reader is reminded to the Appendix for the definition of CVaR. For each candidate allocation vector $\mathbf{PV}$ in the GA population, $\mathrm{CVaR}_\alpha(V;\mathbf{PV})$ is estimated via the MC procedure in Section 3.1. Estimation can be inefficient, requiring multiple AC-OPF solves, and fitness noise can destabilize rankings across generations. To improve stability and speed up convergence, scenario inputs are cached and common random numbers are used within the GA evaluation, with stratified quasi-MC draws held fixed during each fitness assessment.

Stage II: Risk–cost optimization of energy storage systems

Storage is sized/sited to trade voltage-risk reduction against investment cost, while keeping the grid-connected PV allocation fixed at $\mathbf{PV}^\star$ (from Stage I). Let $\mathbf{ES}^p \in \mathbb{R}_+^{n_b}$ denote storage power ratings (MW) and $\mathbf{ES}^e \in \mathbb{R}_+^{n_b}$ storage energy capacities (MWh). The problem is posed as the bi-objective program:

$$(\mathbf{ES}^{p\star}, \mathbf{ES}^{e\star}) = \arg\min_{\mathbf{ES}^p,\mathbf{ES}^e} \Big(J_{II,1}(\mathbf{PV}^\star, \mathbf{ES}^p, \mathbf{ES}^e),\ J_{II,2}(\mathbf{ES}^p, \mathbf{ES}^e) \Big), \tag{11}$$

subject to per-bus capacity constraints for all busses i and total capacity constraints:

$$0 \le ES_i^p \le \bar{b}^{ES}, \qquad 0 \le ES_i^e \le \bar{b}^{E}, \qquad i = 1, \dots, n_b,$$

$$\sum_{i=1}^{n_b} ES_i^p \le \bar{b}^{T_{ES}}, \qquad \sum_{i=1}^{n_b} ES_i^e \le \bar{b}^{T_E}.$$

The first objective is the voltage-deviation tail-risk metric

$$J_{II,1}(\mathbf{PV}^\star, \mathbf{ES}^p, \mathbf{ES}^e) = \mathrm{CVaR}_\alpha\big(V; \mathbf{PV}^\star, \mathbf{ES}^p, \mathbf{ES}^e\big), \tag{12}$$

where $\alpha \in (0,1)$ and V denotes the system-level voltage-deviation random variable obtained from AC-OPF evaluations under uncertain operating conditions (see Appendix A for the CVaR definition). The second objective is the storage investment cost

$$J_{II,2}(\mathbf{ES}^p, \mathbf{ES}^e) = C_{ES}\big(\mathbf{ES}^p, \mathbf{ES}^e\big), \tag{13}$$

computed from the installed storage power and energy ratings. Note that the storage energy capacities $\mathbf{ES}^e$ are post-processed and finalized in Section 3.3 after the dedicated-PV sizing in Stage III, to ensure energy adequacy, i.e., sufficient daily stored energy, under the chosen charging architecture. The technical risk objective $J_{II,1}$ and the expected costs objective $J_{II,2}$ are estimated via the MC engine restricted to PV-deficit periods (night/low-irradiance) to focus on storage effectiveness. The two-way efficiency of the ESs is assumed to be 90%, so that 10% of the energy is lost during charging and discharging, and a depth of discharge of 100% is considered in an optimistic view, with SoC dynamics linking $\mathbf{ES}^p$ and $\mathbf{ES}^e$ (see Section 3.3). Note that this is an idealized assumption, and adopting a more accurate battery model, e.g., efficiency dependent on power and temperature, and a less optimistic discharge window, e.g., 80%–90%, would affect the numerical results, but not the proposed three-stage framework. The solution is a Pareto set explored with a multi-objective evolutionary algorithm, e.g., NSGA-II, or via an ϵ-constraint to meet budget targets.

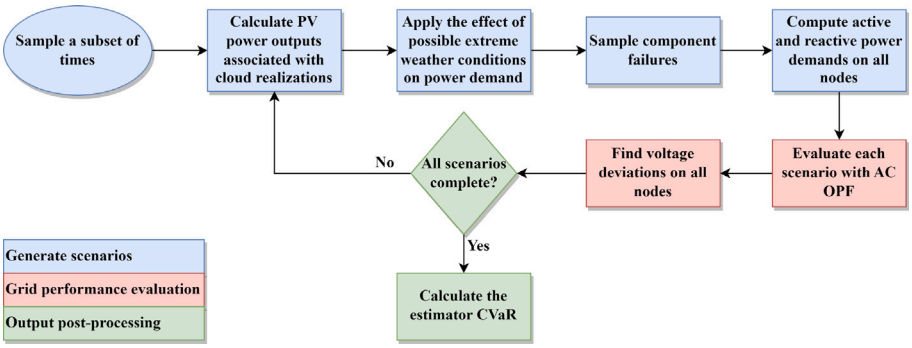


Fig. 3. Flowchart of the Monte Carlo simulator for computing the network voltage deviation risk.

Stage III: Optimal investment on dedicated PV systems

Dedicated PV systems are introduced as a distinct architectural choice in the optimization framework and contribute to the ES state-of-charge but do not inject power directly into the AC network. This decoupled charging configuration separates two planning roles: grid-connected PV is sized/sited in Stage I to shape the grid net injections under AC-OPF constraints, whereas dPV is sized in Stage III to improve storage energy adequacy and availability. This separation is consistent with prior distribution-planning formulations where storage sizing and siting are optimized as a grid-support decision, rather than being treated solely as a passive by-product of PV installation (Nazaripouya et al., 2015; Gupta and Sossan, 2023). The objective of this stage is to achieve the highest amount of successful operation of ESs (which aim to reduce the risk of high voltage deviations) with the least amount of investment cost spent on dedicated PV systems.

The optimization problem solved by the NLP algorithm is:

$$dPV_i^{\star} = \begin{cases} \arg\min_{dPV_i \in \mathbb{R}} \left(J_{III,i}, \text{ if } ES_i^e > 0 \right) \\ 0, \quad \text{if } ES_i^e = 0 \end{cases} \tag{14}$$

subject to:

$$0 \le dPV_i \le b_i^{dPV}, \quad i = 1, \ldots, n_b \tag{15}$$

where $dPV_i^{\star}$ is the optimal size of a dedicated PV system on bus i, which minimizes the objective function defined as $J_{III,i}(dPV_i) = \frac{dPV_i}{R_i^{ES_i}}$, i.e., the ratio of the capacity of the dedicated PV system and its reliability $R_i^{ES_i}$. The threshold b_i^{dPV} represents the maximum allowable dedicated PV capacity in each node (proportional to the maximum investment budget dedicated to enhancing the sustainability of each node). This optimization is performed for each bus individually rather than considering the entire grid simultaneously, and the computational cost is largely reduced. It is also assumed that the ES can store all the amount of energy produced by the dedicated PVs. The resultant $\mathbf{dPV}^{\star}$ vector is the collection of all $dPV_i^{\star}$ for $i = 1, \ldots, n_b$. Obviously, no dedicated PVs are needed on buses without ESs.

Reliability score

A reliability R_i is defined as the probability that the amount of power required by the ES system on the ith bus is met. This score is estimated via the MC method adopting the indicator function $I_{SOC,i}^j$, the indicator function assumes a value equal to 1 when the State-of-Charge of ES installed on bus i satisfies the amount of power required to satisfy the daily load profile of the jth scenario, otherwise its value is zero. The amount of power required by the ESs is obtained by simulating their charging/discharging patterns over the 24 h of a simulated day, which requires solving a sequence of 24 AC-OPFs. Once the required ES power profile is obtained, the estimator of the ESs reliability is computed as follows:

$$R_i^{ES_i} = \frac{1}{n_{mc}} \sum_{j=1}^{n_{mc}} I_{SOC,i}^j, \quad i = 1, \ldots, n_b \tag{16}$$

The procedure to estimate the objective function of Eq. (14) is as follows:

Scenario generation: A random day j is sampled and the environmental–operational variables for 24-hours (t_i $i = 1, \ldots, 24$) is generated accordingly.

Simulate dedicated PV production: The energy produced by a dedicated PV system is calculated from the total solar irradiance, AC-OPFs solved, and the resulting hourly energy injections required by storage is saved. The state of charge, SOC_i^+, is computed as follows:

$$SOC_i^+ = \int_{t_{rise}}^{t_{sunset}} P_{dPV_i}(t')dt' \approx \sum_{t=1}^{n_k} \Delta_t P_{dPV_i}(t_k) \tag{17}$$

Simulate the ES energy discharge overnight: The samples for the night hours are used to calculate the power output of the ES. For each hour of the night, the ES power injections at each node are obtained by solving the AC-OPF, and the required state-of-charge is computed as follows:

$$SOC_i^- = \int_{t_{sunset}}^{t_{rise}} P_{ES_i}(t')dt' \approx \sum_{k=1}^{n_k} \Delta_t P_{ES_i}(t_k) \tag{18}$$

Reliability calculation: The energy discharge identified at step 2 is subtracted from the daily energy charged computed at step 1. If the battery has sufficient energy stored to meet the required energy obtained at step 2, the indicator function used in Eq. (16) becomes:

$$I_{SOC,i}^j = \begin{cases} 1, \text{if } SOC_j^+ \ge SOC_j^- \\ 0, \text{otherwise} \end{cases} \tag{19}$$

The above steps are repeated for n_{mc} random days to obtain an estimate of the ES reliability score and optimal dedicated PV system size for each bus, individually.

3.3. Energy storage capacity sizing

The ESs are assumed to follow a cyclic charge and discharge pattern daily. The energy storage capacities of the ESs are calculated after finding the optimal sizing of dedicated PV systems:

$$ES_i^e = dPV_i \cdot \max_{d \in \{1,2,\ldots,365\}} a_{id}, \quad i = 1, \ldots, n_b \tag{20}$$

where ES_i^e represents the energy storage capacity of the ES on the ith bus, and a_{id} represents the expected energy stored per day j on bus i. ES^e is a vector containing all the values for individual ES_i^e, defining the energy storage capacities and locations of the ESs.

3.4. Carbon tax pricing calculation

The application of Carbon Tax is growing globally to support the reduction of CO_2 gas emissions, one of the biggest contributors to global warming (Anderson et al., 2016). Various Carbon Tax schemes have been proposed and applied worldwide (Ramstein et al., 2019). Here, a Carbon Tax scheme is proposed based on payback period calculation. Such Carbon Tax should allow an investment made in an environmentally friendly project to pay for itself within its warranted period, t_M. The proposed Carbon Tax, CT [€/tonne], is defined as:

$$CT = \frac{C_{\text{inv}} - \int_{t=0}^{t_M} S_{\text{rc}}(t')dt'}{\int_{t=0}^{t_M} R_{\text{CO}_2}(t')dt'} \tag{21}$$

where C_{inv} is the investment cost of the project [€]; $S_{\text{rc}}(t)$ is the instantaneous savings from reduced running costs [€], and therefore $\int_{t=0}^{t_M} S_{\text{rc}}(t')dt'$ represents the cumulative savings until the predefined period t_M [years]; and $R_{\text{CO}_2}(t)$ represents the instantaneous reduction in the emission of CO_2 gas [tonnes], and $\int_{t=0}^{t_M} R_{\text{CO}_2}(t')dt'$ the cumulative CO_2 reduction. The economic feasibility of an ES investment depends on two main parameters: the output power capacity of PV systems and energy storage capacity.

According to Mongird et al. (2019), the cost of such systems is 318,160 [€/MWP] and 305,040 [€/MWh], respectively. On the other hand, the investment cost of a PV system is 700,000 [€/MWP] (Jäger-Waldau et al., 2019). The O&M cost of the distributed generators only depends on the capacity (cost of cleaning and routine checks) and is taken as 20 [€/MWP] and 10.6 [€/kW] per year for PVs and ESs, respectively (Mongird et al., 2019; Enbar et al., 2016; Energy Information Administration, 2020). Hence, the hourly O&M costs of PVs and ESs become 2.28 [€/h] and 1.21 [€/h] per MW capacity installed, respectively. and the cost $f_{\text{O\&M}}(x)$ in Eq. (3) comprises the cost $\sum_j 2.28 \cdot \text{PV}_j$ [€/h] for the photovoltaic panels, $\sum 1.21 \cdot \text{ES}_j$ [€/h] for the ESs, and 1343.4 [€/h] for the three traditional thermal power generators. The fuel cost proportional to the power output, only attributable to the conventional generators, is $f_{p,i}(x) = \sum 122.84 \cdot p_i$ [€/h], which is consistent with the fuel costs of petroleum generators operated by the Electrical Authority of Cyprus.

3.5. Hardware specifications and software used

A desktop computer with a 3.4 GHz CPU, a 64-bit operating system, and 32 GB RAM is used for the MC simulations and GA optimizations. The optimizers are executed via Matlab's *ga* and *fminbnd* functions (Version, 2022), whilst the power system AC-OPF runs on Matpower (Zimmerman et al., 2010). The uncertainty quantification is performed using *OpenCossan* software (Patelli et al., 2016).

3.6. Limitations of the approach

In the context of discussing future developments, it is important to acknowledge that the proposed approach is susceptible to certain limitations attributed to simplifications and underlying assumptions. Specifically, this framework may not leverage the full potential of surplus energy within the Energy Storage Systems (ES). The current framework lacks the incorporation of advanced control strategies for harnessing the added flexibility afforded by distributed energy storage systems. This could involve the utilization of optimal control theory and analogous methodologies to optimize energy management. However, the investigation of advanced control algorithms to improve the exploitation of ES and PVs was beyond the scope of this work. Additionally, owing to certain simplifying assumptions, the framework overlooks energy losses stemming from the storage and conversion of energy generated by PV systems. These considerations could have a significant impact on the viability and profitability of the grid and are worth consideration for future developments.

Table 1
Parameters of the Poisson distribution modeling the failure events (λ_i), and parameters of the (truncated) normal distribution, $\mathcal{N}(\mu_{\tau_i}, \sigma_{\tau_i})$, modeling the duration of the event.

Comp. type	ID	λ_i [event/year]	μ_{τ_i} [h]	σ_{τ_i} [h]
Line	8	5	3	0.5
Line	18	4	2	0.5
Line	30	3	2	1
Line	42	4	3	1
Gen.	29	2	4	1

4. Case study

The proposed methodology is tested on the 35-bus North Cyprus power grid (as of 2009), the data of which is gathered officially from the Cyprus Turkish Electrical Authority. The high-voltage transmission system includes three thermal power plants and a peak total active and reactive demands of 267.1 [MW] and 129.7 [MVAr], respectively. Maximum and minimum voltage deviations per node are set to 0.9 and 1.1 [p.u.]. Three geographical regions named A, B, and C with different solar irradiance and cloudiness characteristics have been created as shown in Fig. 4.

4.1. Simulation parameters

The active and reactive power demand are sampled from a truncated normal distribution with 1-hour resolution and normalized using the annual peak values measured by the Cyprus Turkish Electrical Authority for each bus. The heat wave events are sampled from Poisson distribution with occurrence rate $\lambda_E = 5$ days/year, leading to an inflation of the total power demand of 10% during these events (due to additional cooling).[1] Hourly samples of the total irradiance, i.e., clear sky component less the cloud coverage effect (Cangul et al., 2023), are generated conditionally on the geographical region A, B, and C. The mean value of total irradiance for regions B and C is reduced by 5 and 10 [W/m^2], respectively. The distribution parameters for the component failure events are defined based on expert-based opinion and summarized in Table 1. Example of the yearly nominal power demand, clear-sky irradiance, and total irradiance (including cloud effects) generated by the proposed Monte Carlo simulator are shown Figs. 16 in 19.

4.2. Uncertainty propagation and convergence analysis

Convergence analyses are conducted to identify the smallest number of samples that guarantee the correct ranking of different PVs. To further stabilize the risk estimation, a probabilistic level $\alpha = 0.35$ is selected when computing the risk scores, i.e., 65% of the worst-case scenarios are used to estimate the risk. This relatively low α value avoids discarding too many samples and stabilizes the estimate of the risk calculations. Nonetheless, it focuses only on relatively high-stress scenarios for the North Cyprus network.

The convergence of the objective functions is analyzed for twenty candidate solutions of PV, ES, and dedicated PV randomly generated according to given capacity constraints for all the buses $i \in \{1, \dots, n_b\}$ and subject to the total capacity linear inequality constraint $0 \leq \text{PV}_T \leq 110$. The risk is compared using up to $n_{mc} = 4000$ samples, and the results are shown in Fig. 5. A fair compromise between accuracy and practicality is obtained with $n_{mc} = 250$ samples for the optimization of PV and ES, whereas $n_{mc} = 500$ is chosen for dPV. Each MC sample used for evaluating PV and ES is defined by generating a realization of each of the 110 input parameters of the model ($n_{\text{input}} = 110$) as summarized in Table 2. Fig. 5 presents the results of the convergence analysis.

[1] Heat wave events are studied with daily resolution, i.e., if there is a heat wave, it effects the whole day (or 24 h).

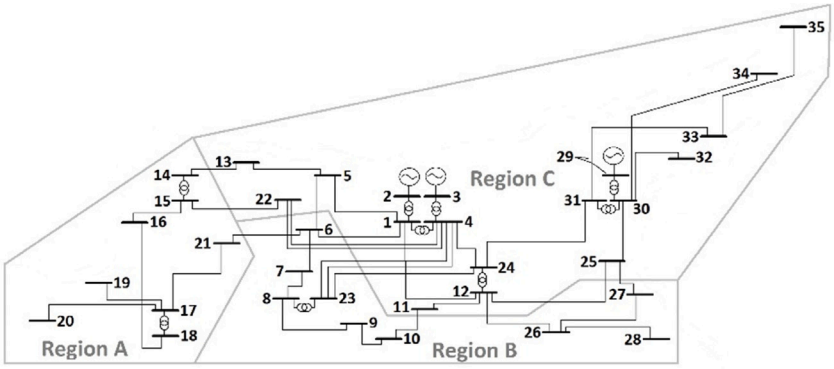
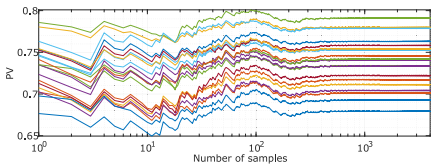
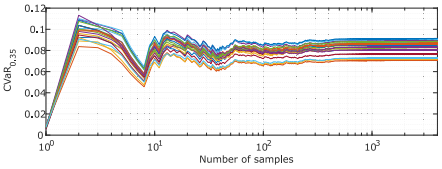


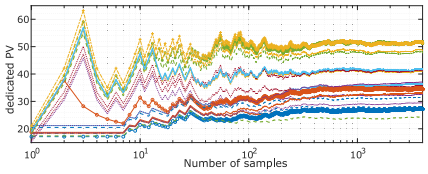
Fig. 4. The 35-bus North Cyprus power grid with 3 different meteorological regions.



(a) Stage I: Risk of voltage deviation for 20 PV allocations.



(b) Stage II: Risk of voltage deviation $CVaR_{0.35}$ for 20 ES allocations.



(c) Stage III: Expectation of the objective function for 20 dedicated PV scenarios

Fig. 5. Convergence analysis of the objective functions in stages I (a), II (b), and III (c) for 20 random configurations, i.e., the design variables. Note that ranking between the 20 scenarios stabilizes for a relatively low number of scenarios.

Table 2
Input parameters for the voltage profile on the 35-bus North Cyprus power grid.

Input parameter	Physical quantity
1 to 35	Active power demand at each node [0, 38.2] [MW]
36 to 70	Reactive power demand at each node [0, 18.5] [MVAr]
71 to 75	Failure indicator for branches 8, 18, 32, 40, and generator 3
76 to 110	Relative PV power generation per 1 MWP capacity

4.3. Sensitivity analysis

Sensitivity analysis aims to identify which uncertain input parameters have the greatest effect on the Conditional Value at Risk of voltage deviation. Two allocation vectors of PV and ES, are defined for this analysis, where PV_i and ES_i^p are set to 10 for all nodes. Morris and variance-based sensitivity analyses, detailed in the Appendix, are employed. Morris analysis assesses the average risk change from a perturbation (Δ) in each input, with Δ set to 0.05 and using 100 samples. The resulting mean and standard deviation of the elementary effects, denoted as EE_μ and EE_σ, are plotted in Fig. 6.

According to both sensitivity analysis methods, the key buses contributing to model uncertainty are buses 5, 8, 28, and 35. An increment in the active power demand at buses 5, 8, and 28 significantly reduces the voltage risk, while the PV power output at buses 16 and 35 increases the risk of large voltage deviation. This can be explained by examining the voltage profile in the original grid, which is almost always above one per unit. Hence, higher power consumption reduces the CVaR of voltage deviation, while the generation of more active power from PVs increases it. Also, bus 35 has the lowest average energy demand, plus it is weakly connected to the rest of the grid. This explains the pronounced effect on the risk of voltage deviations on the nearby buses. This analysis highlights that poorly managed or excessive investment in PV generators can adversely impact transmission grids by jeopardizing stability, resilience, and the overall voltage profile. Long-term voltage stability concerns associated with large-scale PV have, in fact, motivated recent developments in risk-aware planning (Munkhchuluun et al., 2020) and probabilistic risk assessment for transmission systems (Nazir and Bollen, 2024).

4.4. Optimization results

The parameters used in the optimization are summarized in Table 3. Keeping in mind that the solar PV generators are uncontrollable, $b_u^{T_{PV}}$ is selected as 110 [MWP] so the total possible amount of solar PV power generation can never exceed the total active power demand in the system to prevent any system failure due to excessive power injection. For the initial setting of the framework parameters, a preliminary simulation analysis is performed on the North Cyprus power grid without any PVs or ES installed. A safety threshold value of 0.05 [p.u.] is selected for the voltage deviations, and 250 Monte Carlo samples are used to represent one year. AC-OPFs are run for these samples, i.e., one power flow solution for each sample. Among these scenarios, only 36% achieved a voltage profile within the safety threshold of 0.05 [p.u.] Hence, the results strongly support the need for voltage improvements and risk minimization strategies. Moreover, these results are used to

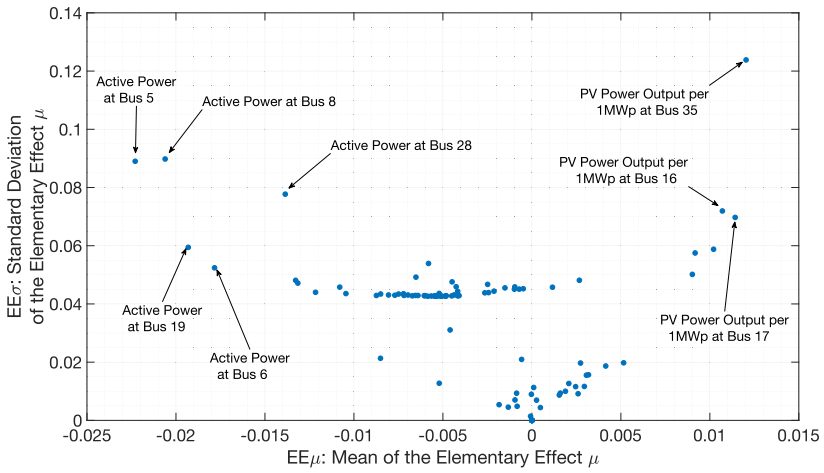


Fig. 6. Morris analysis: EE_{μ} vs. EE_{σ}. Effect of input perturbation on the voltage deviation risk.

Table 3
Optimization parameters for stages I, II and III.

Parameter	Stage		
	I	II	III
Algorithm	GA	GA	NLP
Objective function	J_I	$J_{II,1}, J_{II,2}$	J_{III}
b_u	100 MWP	100 MW	100 MWP
$b_u^{T_{PV}}$	110 MWP	N/A	N/A
n_b	35	35	1
n_{pop}	200	200	N/A
ec	10	10	N/A
co	0.8	0.8	N/A

define an α value for the $CVaR$ calculations, which is set to $\alpha = 0.35$ to focus on the 65% of the most severe voltage deviation samples when computing the tail expectation (risk).

4.4.1. Stage I: Risk-based optimization PV

The GA-based search for the optimal allocation of grid-connected PV generators required approximately 21 h and 51 generations to converge. The resulting siting and sizing are reported in Tables 4 5. In the baseline case without PV, the risk metric $CVaR_{0.35}$ equals 0.0743. Integrating a total PV capacity of 110.5 MWp reduces this value to 0.0421, corresponding to a 43% improvement. Notably, two-thirds of the installed PV capacity is allocated to Bus 34. This outcome reflects the relatively high series resistances of the transmission lines connected to Bus 34, which tend to amplify voltage drops when power is transferred. Concentrating generation at this location therefore mitigates voltage deviations across the wider system, although Bus 34 itself experiences a higher local voltage level compared to the original no-PV case.

4.4.2. Stage II: Risk-cost optimization of ESs

The multi-objective GA optimization for finding the optimal distribution of ES took about 19 [h] and 107 generations to complete. Fig. 7 shows the Pareto front obtained by the multi-objective optimization.

The two objective functions are competing against each other, i.e. the risk of voltage deviations reduces with the addition of batteries, but this leads to a higher investment cost. Three representative solutions on the Pareto front are further inspected:

Model A: Provides the lowest risk $CVaR_{0.35}$ but at the highest investment cost (C_{ES}).
Model B: Represents a balanced trade-off between risk reduction and cost.
Model C: Minimizes investment cost C_{ES} but is associated with the highest operational risk.

The allocation vectors associated with the three models are summarized in Table 4. Note that nodes resulting in small capacity values have been lumped. The CVaR of voltage deviation values obtained by models A, B, and C are 0.0594, 0.0748, and 0.0923, respectively, while the CVaR of voltage deviation with no ES installed is 0.0938. The percentage improvements of the three solutions are, therefore, 37%, 20%, and 2%, respectively. Model C is not further analyzed due to its negligible positive impact on the risk metric and its high similarity to the original grid without distributed generators. For both of the selected solutions, the majority of PV and ES installations are connected to Bus 34 for the same reasons explained in the previous session for the PV sizing and siting.

4.4.3. Stage III: Optimal dPV and ES capacity sizing

To optimize the siting and sizing of dedicated PV systems, the ES are added to the test case according to the $ES^{\star}$ vectors identified for models A and B. The optimization performed by NLP required about 17 [h] per model. The energy storage capacities are then calculated for both models using Eq. (18). The results are summarized in Tables 4 5. The dPV results suggest the addition of a total capacity of 84.1 [MWP] for model A and 37 [MWP] for model B and, like for off-grid PVs and ES, a very high proportion of dPV systems are also installed on Bus 34. These solution of Eq. (18) assure that the ES have enough capacity to store all the energy generated by the dedicated PV systems, i.e., no solar energy produced is wasted. The energy storage capacity of an ES is calculated by multiplying the normalized maximum daily solar PV production of dedicated PV system obtained over a period of a year by the size of the respective dedicated PV system, see Eq. (20).

4.5. Analysis of the results

The obtained results are analyzed from technical, environmental, and economic perspectives. The integration of distributed PV, ES, and dedicated PV systems are analyzed by calculating their impact on the grid parameters and comparing them against the baseline scenario (no PV or ES).

Tables 4 5 show that Buses 11 and 34 are critical for improving the voltage profile of the power grid. The proposed methodology has the flexibility to work with any energy storage system but to provide realistic investment and O&M cost estimates, Lithium-Ion batteries are used due to their longer lifespan compared to other energy storage technologies. The industry generally warrants Lithium-Ion batteries for 10 years, although longer lifespans are expected in practice. Therefore,

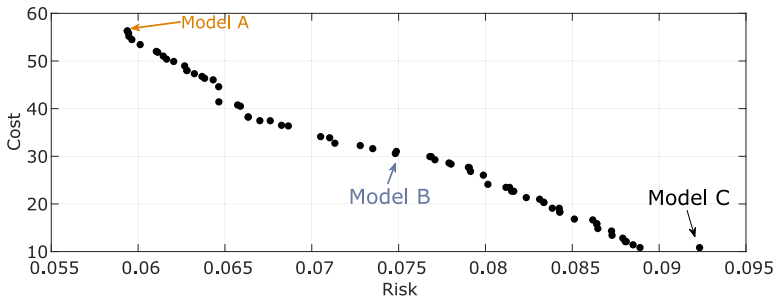
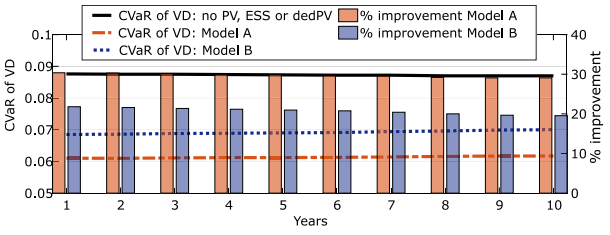


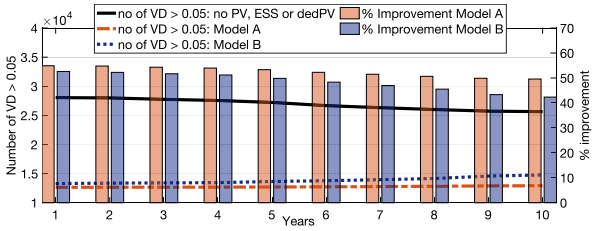
Fig. 7. Pareto front of the Stage II multi-objective optimization for improving voltage profiles. The x-axis reports the voltage-deviation risk objective J_1, Eq. (12), and the y-axis reports the investment cost objective J_2, Eq. (13).

Table 4
Summary of three models and the original case as a baseline for integrating PV systems, ES (power and storage capacities), and dedicated PV systems. Allocated capacities by bus cluster and model. PV in MWp; storage power ES^p in MW; storage energy ES^e in MWh.

Buses	Model	$\mathbf{PV}^\star$	$\mathbf{ES}^{p\star}$	$\mathbf{ES}^{e\star}$	$\mathbf{dPV}^\star$
1–10	Model A	≤1.6	≤0.2	≤2.6	≤0.3
	Model B	≤1.6	≤0.5	≤5.2	≤0.7
	Model C	≤1.6	≤1.0	0.0	0.0
11	Model A	24.7	10.1	107.2	13.6
	Model B	24.7	4.4	63.1	8.0
	Model C	24.7	0.0	0.0	0.0
12–33	Model A	≤1.8	≤0.2	≤2.3	≤0.3
	Model B	≤1.8	≤0.7	≤7.2	≤0.9
	Model C	≤1.8	≤1.5	0.0	0.0
34	Model A	70.2	44.2	537.1	68.1
	Model B	70.2	20.5	168.6	21.9
	Model C	70.2	0.0	0.0	0.0
35	Model A	1.4	0.0	0.0	0.0
	Model B	1.4	0.1	0.4	0.1
	Model C	1.4	1.9	0.0	0.0
1–35	Baseline	0.0	0.0	0.0	0.0



(a) Analysis of CVaR of voltage deviations.



(b) Analysis of voltage deviations greater than 0.05.

Fig. 8. Risk analysis results projected for models A and B over 10 years.

Table 5
Risk and cost summary by model.

Objective	PV risk $J_I(\mathbf{PV}^\star)$	PV-ES risk $J_{\text{II},1}(\mathbf{PV}^\star, \mathbf{ES}^{p\star}, \mathbf{ES}^{e\star})$	ES cost $J_{\text{II},2}(\mathbf{PV}^\star, \mathbf{ES}^{p\star}, \mathbf{ES}^{e\star})$
Model A	0.0421	0.0594	56.2
Model B	0.0421	0.0748	30.9
Model C	0.0421	0.0923	11.0
Baseline	0.0743	0.0743	0

all the analyses are conducted over 10 years to ensure proper operation of each of the components suggested to be installed by the optimizations. The annual degradation of PV panels and Lithium-Ion batteries, as well as the annual power demand growth rate, are taken into consideration. PV panels have a linear degradation of 0.8% per year over 25 years, while the capacity of Lithium-Ion batteries is assumed to depreciate 3% annually. According to the Electricity Authority of Cyprus, the annual growth rate of power demand is expected to be 1%. To estimate the grid's performance through AC-OPFs for 10 years, 1000 MC samples are used, and they account for the degradation of the PV and ES.

4.5.1. Technical analysis

The main output of interest for technical analysis is the CVaR of voltage deviation. The annual expected values of CVaR over a period of 10 years are shown in Fig. 8(a). Similarly, the voltage deviations greater than 0.05 are shown in Fig. 8(b). The Kernel density estimations for voltage deviation for selected buses are shown in Fig. 9. Fig. 10 shows the reliability of the distributed ES defined as the condition of having ample energy to support the power required according to the AC-OPF.

Over time, the risk score CVaR for both Model A and Model B gradually increases as PV and ES degrade and power demand rises. To mitigate this risk, maintenance of degraded components and expansion of PV and ES capacities are recommended. Model A, while more expensive, more effectively reduces the risk of large voltage deviations by increasing total storage power capacity, resulting in improvements ranging from 29.1% to 30.4%. Model B is less costly but presents a higher risk, with improvements between 19.5% and 21.8%. Similarly, the number of voltage deviations exceeding 0.05 also increases over time. Model A outperforms Model B in reducing these deviations, decreasing their occurrence by 49.6% to 54.9%, compared to Model B's range of 42.3% to 52.6%. Model A is thus more effective at lowering both conditional value at risk and the total number of voltage deviations above the maximum displacement threshold of 0.05. To evaluate voltage profile improvements per bus, voltage deviations from unity for all buses in the first year were recorded across all sampled realizations, and corresponding Kernel density estimations were generated. All buses except Bus 34 showed positive improvement, with similar profiles to those observed for Buses 11 and 18. Bus 34 experienced the poorest voltage profile following the addition of grid-connected PV, ES, and dedicated off-grid PV systems. This outcome is attributed to the high amount of generation at Bus 34, which led to increased voltage deviations. Nevertheless, the overall risk to the power grid was reduced. The density estimations remain consistent across different years, with only minor shifts due to component degradation and rising consumer demand. Fig. 10 presents a frequency analysis of ES power availability over a 10-year period. Models A and B exhibit

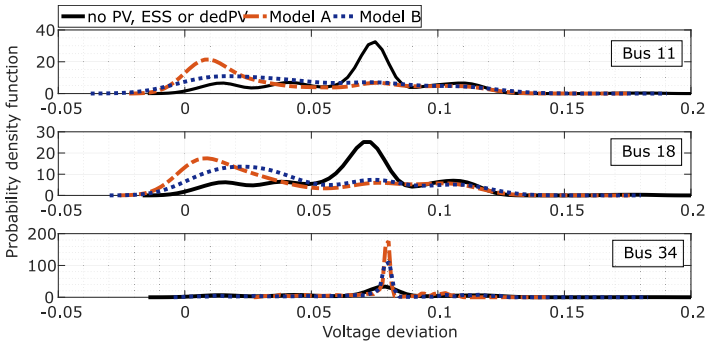


Fig. 9. Kernel density estimations of the voltage deviations for the unity of buses 11, 18, and 34 on year 1.

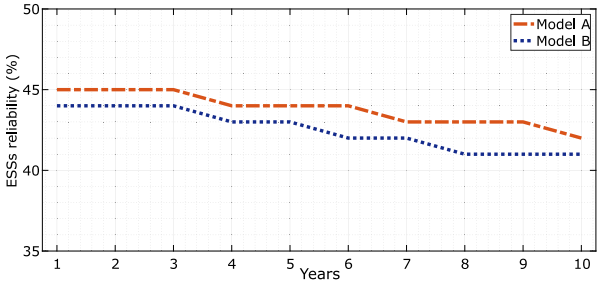


Fig. 10. Reliability of the energy storage units over 10 years for models A and B.

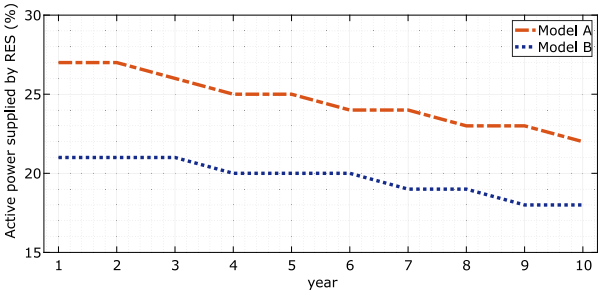


Fig. 11. Total active power demand supplied by RESs over 10 years for Models A and B.

similar battery profiles, with reliability ranging from 45% to 42% and 44% to 42%, respectively.

4.5.2. Environmental analysis

To investigate the environmental effects of models A and B, the total energy share and the corresponding CO_2 emission reductions are shown in Figs. 11 and 12, respectively. The results are illustrated in Fig. 11. For solution A, the RESs provide 27% of the total energy supply in year 1, decreasing to about 22% by year 10. For model B, the RES share drops from 21% in year 1 to 18% in year 10. This decline is driven by gradual RES degradation and increasing power demand over time. Please note that the PV systems are installed at time zero, and no further PV installation occurs over the 10-year period considered. Knowing the energy produced by PV systems with models A and B, we can compute the reduction of energy required by the current power plants burning petroleum and the corresponding reduction of CO_2 emission. Current power plants burning petroleum produce 0.9661517 tons of CO_2 per MWh (Administration, 2020), and the resultant CO_2 emission reduction is shown in Fig. 12. Model A prevents the emission of a total of 2.8M tons of CO_2, while model B saves 2.3 million tonnes over a period of 10 years. This corresponds to the amount absorbed by about 12.9 and 10.7, respectively.

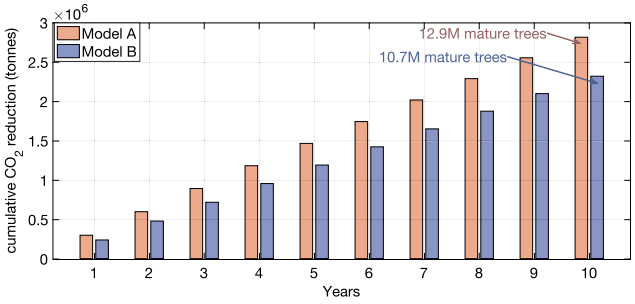


Fig. 12. Cumulative CO_2 reduction over 10 years for models A and B.

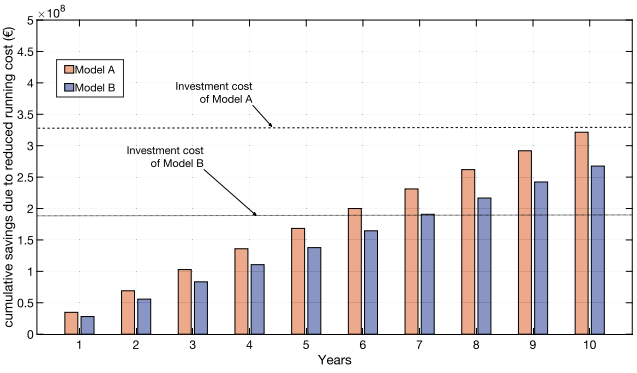


Fig. 13. Cumulative savings from reduced running costs over 10 years for models A and B.

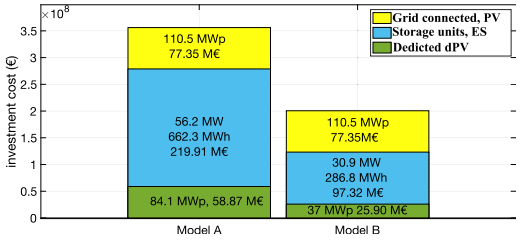


Fig. 14. The investment costs of models A and B.

4.5.3. Economic analysis

This section discusses the economic impact of investment Models A and B. The total investment costs of Models A and B are 356 M€ and 201 M€, respectively. Fig. 14 reports the corresponding breakdown of investment costs by technology, including the installed power and energy ratings of grid-connected PV, energy storage, and dedicated

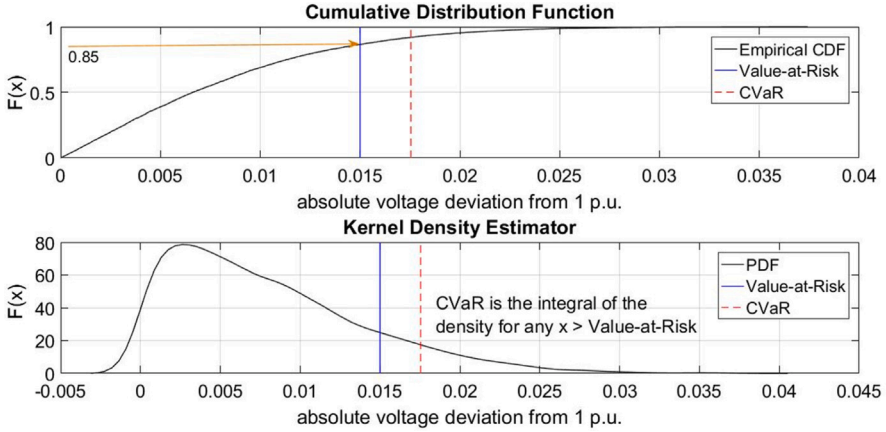


Fig. 15. Example of $CVaR_{\alpha}(V)$, red dashed vertical line, and Value-at-Risk, blue solid vertical line, for the same probabilistic level $\alpha = 0.85$.

PV. It is worth noting that Models A and B share the same grid-connected PV allocation, as expected, as it results from the same optimization problem (Stage I). In contrast, Model A includes a substantially larger share of storage units and dedicated PV, namely 56 MW and 84.1 MWp, respectively, compared to Model B (30.9 MW and 37 MWp, respectively). This is due to the higher-investment solution (and lower voltage-risk) associated to Model A. The integration of DGs into the power grid, despite increasing the overall operational and maintenance costs, reduced the total running costs faced by the grid operator. The cumulative savings over 10 years are estimated and compared to the expected investment costs of the PV and ES units. This results in a saving of 321 M€ for model A and 268 M€ savings for model B. This result is also illustrated in Fig. 13, which shows the cumulative savings of the two investments over 10 years (due to reduced running cost). Note that, Model B pays back its investment cost within approximately 6 years, whereas Model A does not return the investment within the 10-year time frame.

Hence, Carbon Tax of 12.5 €/tonne, calculated using Eq. (21), is needed to make model A economically viable within the 10-year investment horizon. For comparison, the current Carbon Tax per tonne in the EU varies between 117.30 € in Sweden, 45 € in France, 15 € in Spain, and 0.93 € in Ukraine, as of April 2022 (Bray, 2022). The investment, as suggested by Model B, is economically viable independently of the Carbon Tax.

The difference in the payback period between the two models is primarily attributable to the different sizing of the energy storage units. In the present analysis, ES is not modeled to generate additional arbitrage revenues or ancillary-service income and, accordingly, does not directly drive annual running-cost savings or CO_2 emission reductions. Nonetheless, ES enables higher PV penetration and improves overall power quality, stabilizes the voltage profile, and enhances grid robustness. Overall, Model A delivers a better technical and environmental performance than Model B, but with a worse economic outcome. Therefore, investment planning entails a compromise between the reduction of technical voltage-related risks, environmental targets, and economic performance. The final decision should reflect both system-level technical priorities and the economic constraints of the investor, e.g., the electrical authority. Also note that in the present analysis, the running-cost savings are mainly driven by reduced dispatch of conventional generators (and thus reduced fuel costs) because PV injections lower net demand in the AC-OPF. Storage is not modeled to generate additional arbitrage revenues or ancillary-service income, and it is primarily valued here for voltage-risk mitigation and for enabling higher PV penetration.

5. Discussion: Limitations, management, policy implications, and future directions

A combination of public and private investments in large-scale renewable sources presents an attractive strategy to rapidly decarbonize electrical grids. Our results indicate that investing in photovoltaic generators, energy storage systems, and dedicated PV systems can significantly reduce the risk of voltage profile instabilities and CO_2 emissions. Furthermore, these investments offer a reasonably short payback period. However, one challenge is the potential generation of surplus energy that may not be fully utilized, necessitating the deployment of large-scale storage units. Efficient utilization of this energy surplus depends on the grid's specific location and may include long-term storage solutions, seawater desalination (particularly in areas with water scarcity), electric mobility (such as vehicle-to-grid and grid-to-vehicle concepts), hydrogen production, or control policies that enable the storage units to discharge only during specific conditions, like cloudy weather. Maximizing the efficient use of surplus energy can have a positive economic impact. Nevertheless, an over-investment in renewable generators, if not managed properly, can lead to voltage instabilities and severe power quality issues. Therefore, the optimal allocation and control of renewable sources must consider the increasing digitalization of the power grid, the electrification of the transportation network, and the essential collaborative efforts to reduce the overall carbon footprint while meeting future climate and resilience goals. New energy exchange policies between distributed renewable generators and storage units (both stationary and mobile, e.g., electric vehicles) should be further investigated. To enable real-world deployment, power quality indicators such as voltage profile, frequency stability, peak shaving, and valley filling should be systematically evaluated, ideally through high-fidelity digital twins and detailed simulation studies. In addition, market-coupled ancillary services (e.g., primary frequency regulation with ESS) can substantially influence system economics and should be explicitly incorporated in future research.

From a management and policy perspective, this work and its results support the transition from deterministic N-1 planning toward risk-informed frameworks that explicitly account for low-probability and high-impact events, e.g., extreme weather like heat waves. This is consistent with the ongoing shift toward probabilistic risk assessment as a complement to N-1 in Europe. In practice, TSOs and distribution system operators could exploit the risk–cost trade-off solutions produced by the proposed workflow to shortlist candidate portfolios and select one based on budget constraints and a defined risk appetite, rather than relying on a single least-cost solution. For regulators, carbon pricing, or equivalent targeted incentives, can be calibrated to the break-even levels indicated by the economic assessment, prioritizing investments that deliver the largest marginal reduction in voltage-risk per euro. Finally,

connection codes and flexibility markets can be designed to reward storage operations that demonstrably reduce voltage risks, aligning private dispatch incentives with system-level resilience.

6. Conclusions

An efficient and robust method for optimally allocating off-grid decentralized solar photovoltaic generators, energy storage units, and dedicated photovoltaic systems within a power grid has been presented. The proposed approach offers a comprehensive evaluation of investments in photovoltaic and storage units, encompassing technical, environmental, and economic perspectives. Specifically, it enhances the power grid voltage profile by minimizing voltage deviations from unity and focuses on the most critical and risky conditions by optimizing the CVaR of voltage deviation. A 3-Stage multi-objective optimization procedure has been developed to overcome the limitations of existing tools by providing realistic engineering models and simulations for the grid's components and network topology, explicitly considering the impact of uncertainty at manageable computational costs. The method proves to be an effective tool for power system planning, enabling the analysis of different investment strategies to strike the best balance between risk and cost. Additionally, this study demonstrated that even a modest Carbon Tax can make investments in renewable energy economically viable. The paper also showcased the practical application of the proposed methodology for analyzing the lifetime performance of actual power grids, including the assessment of unavoidable uncertainties, the identification of mitigation strategies (due to degradation/ageing and increasing power demand), and the attainment of robust solutions.

CRediT authorship contribution statement

Ozcel Cangul: Writing – review & editing, Writing – original draft, Visualization, Methodology, Data curation, Software. **Roberto Rocchetta:** Writing – review & editing, Writing – original draft, Visualization, Supervision, Methodology, Funding acquisition. **Edoardo Patelli:** Writing – review & editing, Writing – original draft, Supervision, Project administration, Funding acquisition, Conceptualization.

Declaration of competing interest

The authors declare the following financial interests/personal relationships which may be considered as potential competing interests: Roberto Rocchetta reports financial support was provided by Swiss Federal Office of Energy. If there are other authors, they declare that they have no known competing financial interests or personal relationships that could have appeared to influence the work reported in this paper.

Acknowledgment

The authors gratefully acknowledge the support of the Swiss Federal Office of Energy (SFOE), Switzerland for the project "PROPER-Grids: Probabilistic Risk-informed Operational Scheduling for Power Grids" under grant agreement SI/502663.

Appendix A. Conditional Value-at-Risk

The CVaR for large voltage deviations is defined as follows:

$$VaR_\alpha(V) := F_V^{-1}(\alpha), \qquad CVaR_\alpha(V) := \frac{1}{1-\alpha}\int_\alpha^1 F_V^{-1}(\tau)\,d\tau,$$

where F_V^{-1} is the inverse cumulative distribution function of the voltage deviations in per-units, $\alpha \in [0,1]$ is a probabilistic level. The value-at-risk $VaR_\alpha(V)$ is a threshold deviation level that, if exceeded, indicates an unstable/hazardous operational state for the grid. Note that the $CVaR_\alpha(V)$ is the expectation over a portion of the tail of the distribution of V, i.e., it accounts not only for the probability of exceeding the Value-at-Risk but also for the shape of the tails of the V distribution in the region $x > F_V^{-1}(\alpha)$ (see Fig. 15).

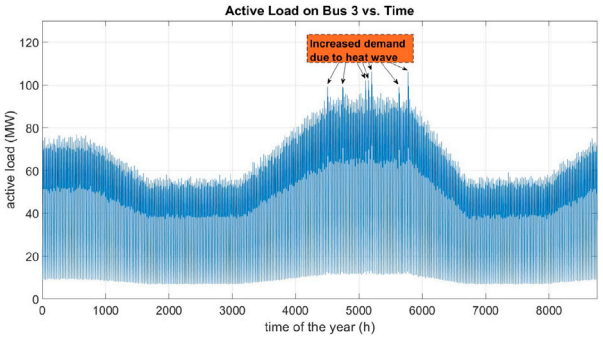


Fig. 16. Active power demand on Bus 3 over 8760 [h] of the year.

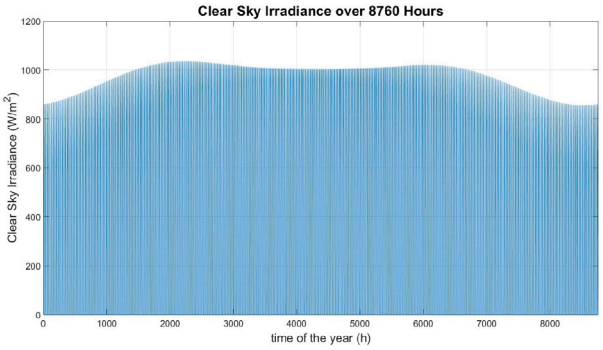


Fig. 17. Clear sky irradiance for Cyprus over 8760 [h] of the year.

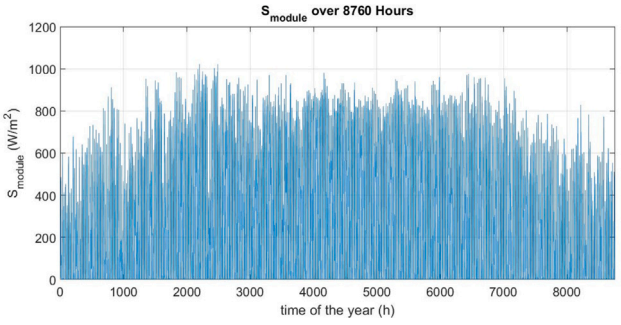


Fig. 18. S_{module} irradiance on Region A over 8760 [h] of a simulated year (after cloud effects are accounted for).

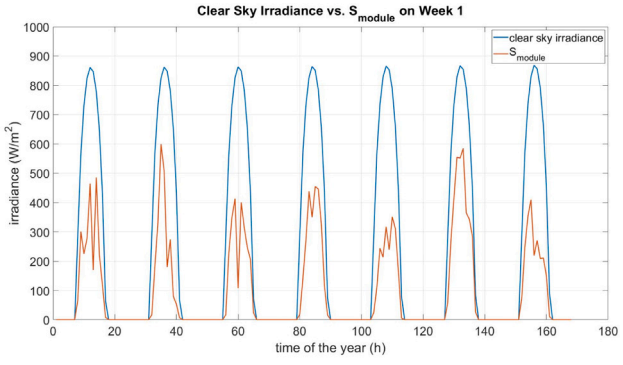


Fig. 19. The clear sky irradiance profile vs. the S_{module} irradiance profile on Region A over the first week of the year.

Appendix B. Sensitivity analysis

The Elementary Effects analysis is a low-computation qualitative screening method that identifies influential input parameters on the model output (Turati et al., 2016). It quantifies the effects of input parameters $X(i)$ on Y using One-At-a-Time incremental ratios (Morris, 1991). The elementary effect $d_i(X_0)$ for input $X(i)$ is calculated as:

$$d_i(X_0) = \frac{Y(X_0(1), \dots, X_0(i) + \Delta, \dots, X_0(K)) - Y(X_0)}{\Delta} \tag{22}$$

A higher $d_i(X)$ indicates a stronger influence. The mean and standard deviation of the elementary effect are EE_{μ_i} and EE_{σ_i}. Morris' method assesses input importance based on these statistics, with high EE_{μ_i} values indicating a strong linear correlation and high EE_{σ_i} values suggesting non-linear effects and parameter interaction. Sobol' indices, also known as first-order sensitivity indices, are variance-based metrics that quantify the impact of input factor variance on output variance (Soboĺ, 1993). The Given Data approach by Soboĺ (1993) efficiently calculates these indices without requiring additional model evaluations. The first-order sensitivity indices, which measure the direct impact of input variations, are defined as:

$$S_i = \frac{V_{X_i}[\mathbb{E}_{X_{\sim i}}[Y|X_i]]}{V[Y]} \tag{23}$$

Here, X_i is the ith input parameter, $X_{\sim i}$ is the matrix of all other input factors, and $\mathbb{E}_{X_{\sim i}}[Y|X_i]$ is the output expectation while X_i is fixed. $V_{X_i}[\cdot]$ is the variance over X_i values, and $V[Y]$ is the total output variance. A higher Sobol' index value signifies a stronger input parameter effect on output variance.

Appendix C. Simulated operational–environmental variables

Figs. 16 to 19 show the resultant graphs of some of the important outputs of the proposed Monte Carlo simulator.

List of abbreviations

DG	Distributed Generators
RES	Renewable Energy Sources
PV	Solar Photovoltaic (Grid-connected)
dPV	Dedicated Solar Photovoltaic (Off-grid)
ES	Energy Storage System
GA	Genetic Algorithm
NLP	Nonlinear Programming
CO_2	Carbon Dioxide
SOC	State-of-Charge
MC	Monte Carlo
CVaR	Conditional Value-at-Risk
AC	Alternating Current
OPF	Optimal Power Flow
O&M	Operations and Maintenance
EE	Elementary Effect
SS	Sizing and Siting

Data availability

Data will be made available on request.

References

Administration, U.E.I., 2020. How much carbon dioxide is produced per kilowatthour of US electricity generation? Freq. Asked Quest. (FAQ).

Akdemir, K.Z., Mongird, K., Kern, J.D., Oikonomou, K., Voisin, N., Burleyson, C.D., Rice, J.S., Zhao, M., Bracken, C., Vernon, C., 2025. Investigating the effects of cooperative transmission expansion planning on grid performance during heat waves with varying spatial scales. Appl. Energy 378, 124825.

Aldy, J.E., Stavins, R.N., 2012. The promise and problems of pricing carbon: Theory and experience. J. Environ. Dev. 21 (2), 152–180.

Anderson, T.R., Hawkins, E., Jones, P.D., 2016. CO2, the greenhouse effect and global warming: from the pioneering work of Arrhenius and callendar to today's earth system models. Endeavour 40 (3), 178–187.

Bahrami, M., Vakilian, M., Farzin, H., Lehtonen, M., 2023. A CVaR-based stochastic framework for storm-resilient grid, including bus charging stations. Sustain. Energy Grids Netw. 35, 101082. https://doi.org/10.1016/j.segan.2023.101082.

Bawazir, R.O., Cetin, N.S., 2020. Comprehensive overview of optimizing PV-DG allocation in power system and solar energy resource potential assessments. Energy Rep. 6, 173–208.

Bray, S., 2022. Carbon Taxes in Europe. Tax Foundation, NewYork, NY, USA.

Cadini, F., Agliardi, G.L., Zio, E., 2017. A modeling and simulation framework for the reliability/availability assessment of a power transmission grid subject to cascading failures under extreme weather conditions. Appl. Energy 185, 267–279.

Cangul, O., 2021. Robust Allocation of Decentralized Photovoltaic and Energy Storage Systems in a Power Grid under Uncertainty (Ph.D. thesis). University of Liverpool.

Cangul, O., Rocchetta, R., Fahrioglu, M., Patelli, E., 2023. Optimal allocation and sizing of decentralized solar photovoltaic generators using unit financial impact indicator. Sustainability 15 (15), 11715.

Carpinelli, G., Noce, C., Russo, A., Varilone, P., Verde, P., 2024. Optimal siting and sizing of battery energy storage systems in unbalanced distribution systems: A multi objective problem under uncertainty. Int. J. Electr. Power Energy Syst. 162, 110316. https://doi.org/10.1016/j.ijepes.2024.110316.

Cervan, D., Coronado, A.M., Luyo, J.E., 2023. Cluster-based stratified sampling for fast reliability evaluation of composite power systems based on sequential Monte Carlo simulation. Int. J. Electr. Power Energy Syst. 147, 108813.

Department of Meteorology, Republic of Cyprus, 2022. Meteorological reports. (Accessed 20 July 2022).

Ehsan, A., Yang, Q., 2018. Optimal integration and planning of renewable distributed generation in the power distribution networks: A review of analytical techniques. Appl. Energy 210, 44–59.

Enbar, N., Weng, D., Klise, G.T., 2016. Budgeting for Solar PV Plant Operations & Maintenance: Practices and Pricing. Tech. Rep., Sandia National Lab.(SNL-NM), Albuquerque, NM (United States).

Energy Information Administration, U., 2020. Capital cost and performance characteristic estimates for utility scale electric power generating technologies.

ENTSO-E, 2023. Biennial Progress Report on Operational Probabilistic Coordinated Security Assessment and Risk Management. Tech. Rep., ENTSO-E, Accessed 2025-12-09.

ENTSO-E, 2025. Factual Report on the Grid Incident in Spain and Portugal on 28 April 2025. Tech. Rep., European Network of Transmission System Operators for Electricity (ENTSO-E), (Accessed 09 December 2025).

Erdiwansyah, Mahidin, Husin, H., Nasaruddin, Zaki, M., Muhibbuddin, 2021. A critical review of the integration of renewable energy sources with various technologies. Prot. Control. Mod. Power Syst. 6, 1–18.

Garcia-Sanz, M., Marden, M., Cvetkovic, I., Oh, H., LoCicero, E., Khalid, S., 2025. Grid fragility, blackouts, and control co-design solutions. Adv. Control. Appl.: Eng. Ind. Syst. 7 (3), e70022.

Gupta, R., Sossan, F., 2023. Optimal sizing and siting of energy storage systems considering curtailable photovoltaic generation in power distribution networks. Appl. Energy 339, 120955.

Hadidian-Moghaddam, M.J., Arabi-Nowdeh, S., Bigdeli, M., Azizian, D., 2018. A multi-objective optimal sizing and siting of distributed generation using ant lion optimization technique. Ain Shams Eng. J. 9 (4), 2101–2109.

Huiling, T., Jiekang, W., Lingmin, C., Zhijun, L., Fan, W., Kangxing, L., Zhijiang, W., Fangming, Y., Qilin, B., 2021. A control optimization model for cvar risk of distribution systems with PVs/DSs/EVs using Q-learning powered adaptive differential evolution algorithm. Int. J. Electr. Power Energy Syst. 132, 107209.

Inaolaji, A., Wu, X., Roychowdhury, R., Smith, R., 2024. Optimal allocation of battery energy storage systems for peak shaving and reliability enhancement in distribution systems. J. Energy Storage 95, 112305.

Injeti, S.K., Thunuguntla, V.K., 2020. Optimal integration of DGs into radial distribution network in the presence of plug-in electric vehicles to minimize daily active power losses and to improve the voltage profile of the system using bio-inspired optimization algorithms. Prot. Control. Mod. Power Syst. 5, 1–15.

Iqbal, H., Stevenson, A., Sarwat, A.I., 2025. Impact analysis and optimal placement of distributed energy resources in diverse distribution systems for grid congestion mitigation and performance enhancement. Electronics 14 (10), https://doi.org/10.3390/electronics14101998.

Jäger-Waldau, A., et al., 2019. PV Status Report 2019. Publications Office of the European Union, Luxembourg, pp. 7–94.

Jain, S., Kalambe, S., Agnihotri, G., Mishra, A., 2017. Distributed generation deployment: State-of-the-art of distribution system planning in sustainable era. Renew. Sustain. Energy Rev. 77, 363–385.

Javadi, M.S., Gough, M., Mansouri, S.A., Ahmarinejad, A., Nematbakhsh, E., Santos, S.F., Catalão, J.P., 2022. A two-stage joint operation and planning model for sizing and siting of electrical energy storage devices considering demand response programs. Int. J. Electr. Power Energy Syst. 138, 107912.

Khorramfar, R., Mallapragada, D., Amin, S., 2025. Power-gas infrastructure planning under weather-induced supply and demand uncertainties. European J. Oper. Res. https://doi.org/10.1016/j.ejor.2025.08.049.

Kow, K.W., Wong, Y.W., Rajkumar, R.K., Rajkumar, R.K., 2016. A review on performance of artificial intelligence and conventional method in mitigating PV grid-tied related power quality events. Renew. Sustain. Energy Rev. 56, 334–346.

Li, C., Dai, J., Zhu, S., Guo, R., Liu, Z., Jiang, Y., Tian, S., Wen, Y., 2025. Credible capacity evaluation of virtual power plants considering wind and PV uncertainties. Sci. Rep. 15 (1), 41976.

Li, J., Wang, X., Wang, Z., Song, Z., 2025. Conditional distributionally robust dispatch for integrated transmission-distribution systems via distributed optimization. Int. J. Electr. Power Energy Syst. 166, 110559.

Li, R., Wong, P., Wang, K., Li, B., Yuan, F., 2020. Power quality enhancement and engineering application with high permeability distributed photovoltaic access to low-voltage distribution networks in Australia. Prot. Control. Mod. Power Syst. 5 (1), 1–7.

Li, J., Zhang, Z., Shen, B., Gao, Z., Ma, D., Yue, P., Pan, J., 2020. The capacity allocation method of photovoltaic and energy storage hybrid system considering the whole life cycle. J. Clean. Prod. 275, 122902.

Lim, K.Z., Lim, K.H., Wee, X.B., Li, Y., Wang, X., 2020. Optimal allocation of energy storage and solar photovoltaic systems with residential demand scheduling. Appl. Energy 269, 115116.

Lin, S., Liu, S., Zhu, H., 2022. Risk-aware learning for scalable voltage optimization in distribution grids. Electr. Power Syst. Res. 212, 108605. https://doi.org/10.1016/j.epsr.2022.108605.

Liu, B., Hou, Y., Luan, W., Liu, Z., Chen, S., Yu, Y., 2023. A divide-and-conquer method for compression and reconstruction of smart meter data. Appl. Energy 336, 120851.

Liu, Y., Zhang, X., Ma, Z., Ren, W., Xiao, Y., Xu, X., Liu, Y., Liu, J., 2025. Risk-aware scheduling for maximizing renewable energy utilization in a cascade hydro–PV complementary system. Energies 18 (12), 3109.

Mei, Y., Omidvar, M.N., Li, X., Yao, X., 2016. A competitive divide-and-conquer algorithm for unconstrained large-scale black-box optimization. ACM Trans. Math. Softw. (TOMS) 42 (2), 1–24.

Mena, R., Hennebel, M., Li, Y.-F., Ruiz, C., Zio, E., 2014. A risk-based simulation and multi-objective optimization framework for the integration of distributed renewable generation and storage. Renew. Sustain. Energy Rev. 37, 778–793.

Mongird, K., Viswanathan, V., Balducci, P., Alam, J., Fotedar, V., Koritarov, V., Hadjerioua, B., 2019. Energy Storage Technology and Cost Characterization, Report PNNL-28866.

Monteiro, R.V.A., Bonaldo, J.P., da Silva, R.F., Bretas, A.S., 2020. Electric distribution network reconfiguration optimized for PV distributed generation and energy storage. Electr. Power Syst. Res. 184, 106319.

Moradi-Sepahvand, M., Amraee, T., Aminifar, F., Akbari, A., 2023. Coordinated expansion planning of transmission and distribution systems integrated with smart grid technologies. Int. J. Electr. Power Energy Syst. 147, 108859.

Morris, M.D., 1991. Factorial sampling plans for preliminary computational experiments. Technometrics 33 (2), 161–174.

Morsy, B., Hinneck, A., Pozo, D., Bialek, J., 2022. Security constrained OPF utilizing substation reconfiguration and busbar splitting. Electr. Power Syst. Res. 212, 108507.

Mukhopadhyay, B., Das, D., 2020. Multi-objective dynamic and static reconfiguration with optimized allocation of PV-DG and battery energy storage system. Renew. Sustain. Energy Rev. 124, 109777.

Munkhchuluun, E., Meegahapola, L., Vahidnia, A., 2020. Long-term voltage stability with large-scale solar-photovoltaic (PV) generation. Int. J. Electr. Power Energy Syst. 117, 105663.

Nazaripouya, H., Wang, Y., Chu, P., Pota, H.R., Gadh, R., 2015. Optimal sizing and placement of battery energy storage in distribution system based on solar size for voltage regulation. In: 2015 IEEE Power & Energy Society General Meeting. IEEE, pp. 1–5.

Nazir, Z., Bollen, M., 2024. Operational risk assessment of transmission systems: A review. Int. J. Electr. Power Energy Syst. 159, 109995.

Panteli, M., Pickering, C., Wilkinson, S., Dawson, R., Mancarella, P., 2017. Power system resilience to extreme weather: Fragility modelling, probabilistic impact assessment, and adaptation measures. IEEE Trans. Power Syst. PP (99), 1. https://doi.org/10.1109/TPWRS.2016.2641463.

Patelli, E., Ghanem, R., Higdon, D., Owhadi, H., 2016. COSSAN: a multidisciplinary software suite for uncertainty quantification and risk management. Handb. Uncertain. Quantif. 1–69.

Peng, C., Xiong, Z., Zhang, Y., Zheng, C., 2022. Multi-objective robust optimization allocation for energy storage using a novel confidence gap decision method. Int. J. Electr. Power Energy Syst. 138, 107902.

Piansky, R., Gupta, R., Molzahn, D.K., 2025. Optimizing battery and line undergrounding investments for transmission systems under wildfire risk scenarios: A benders decomposition approach. Sustain. Energy Grids Netw. 43, 101838. https://doi.org/10.1016/j.segan.2025.101838.

Popli, N., Davoodi, E., Capitanescu, F., Wehenkel, L., 2024. On the robustness of machine-learnt proxies for security constrained optimal power flow solvers. Sustain. Energy Grids Netw. 37, 101265. https://doi.org/10.1016/j.segan.2023.101265.

Prakash, P., Khatod, D.K., 2016. Optimal sizing and siting techniques for distributed generation in distribution systems: A review. Renew. Sustain. Energy Rev. 57, 111–130.

Prasad, K., Kollu, R., Ramkumar, A., Ramesh, A., 2025. A multi-objective strategy for optimal DG and capacitors placement to improve technical, economic, and environmental benefits. Int. J. Electr. Power Energy Syst. 165, 110491.

Qi, X., Khattak, B.N., Alam, A., Liu, W., 2024. Intelligent optimal sitting and sizing of distributed resources in presence of renewable energy and fuel cells based on reliability and emission factors. Energy Rep. 12, 1080–1093. https://doi.org/10.1016/j.egyr.2024.06.067.

Rahim, S., Wang, Z., Sun, K., Chen, H., 2024. A Wasserstein distributionally robust model for transmission expansion planning with renewable-based microgrid penetration. IET Gener. Transm. Distrib. 18 (17), 2793–2808.

Ramstein, C., Dominioni, G., Ettehad, S., Lam, L., Quant, M., Zhang, J., Mark, L., Nierop, S., Berg, T., Leuschner, P., et al., 2019. State and Trends of Carbon Pricing 2019. The World Bank.

Rinaldi, A., Soini, M.C., Patel, M.K., Parra, D., 2020. Optimised allocation of PV and storage capacity among different consumer types and urban settings: A prospective analysis for Switzerland. J. Clean. Prod. 259, 120762.

Rocchetta, R., Bellè, A., Blazhe, G., 2025. Towards risk-informed transmission grid outage planning. In: Proceedings of the 35th European Safety and Reliability & the 33rd Society for Risk Analysis Europe Conference. pp. 587–594.

Rocchetta, R., Crespo, L.G., 2021. A scenario optimization approach to reliability-based and risk-based design: Soft-constrained modulation of failure probability bounds. Reliab. Eng. Syst. Saf. 216, 107900.

Rocchetta, R., Li, Y., Zio, E., 2015. Risk assessment and risk-cost optimization of distributed power generation systems considering extreme weather conditions. Reliab. Eng. Syst. Saf. 136, 47–61.

Rocchetta, R., Zio, E., Patelli, E., 2018. A power-flow emulator approach for resilience assessment of repairable power grids subject to weather-induced failures and data deficiency. Appl. Energy 210 (C), 339–350. https://doi.org/10.1016/j.apenergy.2017.1.

Rockafellar, R.T., Uryasev, S., et al., 2000. Optimization of conditional value-at-risk. J. Risk 2, 21–42.

Rodríguez, J.A., Anjos, M.F., Côté, P., Desaulniers, G., 2021. Accelerating benders decomposition for short-term hydropower maintenance scheduling. European J. Oper. Res. 289 (1), 240–253.

Shi, J., Qin, J., Li, H., Li, Z., Ge, Y., Liu, B., 2024. Probabilistic power and energy balance risk scheduling method based on distributed robust optimization. Energies 17 (19), https://doi.org/10.3390/en17194894.

Soboĺ, I., 1993. Sensitivity estimates for nonlinear mathematical models. Math. Model. Comput. Exp. 1, 407.

Tillmanns, M., Schöttler, J., Praktiknjo, A., 2026. A review of probabilistic resource adequacy assessments in power systems: Methods, applications, and future challenges. Energy Policy 209, 114924. https://doi.org/10.1016/j.enpol.2025.114924.

Turati, P., Pedroni, N., Zio, E., 2016. Dimensionality reduction of the resilience model of a critical infrastructure network by means of elementary effects sensitivity analysis. In: European Safety and RELiability Conference (ESREL) 2016. pp. 2797–2804.

Version, M., 2022. MATLAB Version 9.12. 0.1927505 (R2022a) Update 1. The Mathworks, Natick, MA, USA.

Wang, J., Song, Y., 2023. Distributionally robust OPF in distribution network considering CVaR-averse voltage security. Int. J. Electr. Power Energy Syst. 145, 108624.

Wang, X., Ying, L., Wen, K., Lu, S., 2022. Bi-level non-convex joint optimization model of energy storage in energy and primary frequency regulation markets. Int. J. Electr. Power Energy Syst. 134, 107408.

Wong, L.A., Ramachandaramurthy, V.K., Walker, S.L., Taylor, P., Sanjari, M.J., 2019. Optimal placement and sizing of battery energy storage system for losses reduction using whale optimization algorithm. J. Energy Storage 26, 100892.

Xiong, K., Di Cao, Zhang, G., Chen, Z., Hu, W., 2023. Coordinated volt/VAR control for photovoltaic inverters: A soft actor-critic enhanced droop control approach. Int. J. Electr. Power Energy Syst. 149, 109019.

Ye, J., Song, J., Ma, H., Yang, Q., Li, D., Yin, W., et al., 2025. Resilient planning for battery and hydrogen energy storage in power systems against extreme heatwave events. J. Energy Storage 139, 118850.

Zhang, X., Chen, H., Xu, Y., Li, W., He, F., Guo, H., Huang, Y., 2017. Distributed generation with energy storage systems: A case study. Appl. Energy 204, 1251–1263.

Zhang, C., Xu, Y., Siano, P., Wang, Z., Mishra, S., Caire, R., Hill, D., 2025. Editorial - advances in Volt/Var control for active distribution networks with high-level intermittent renewable energy resources. Int. J. Electr. Power Energy Syst. 164, 110423.

Zhou, S., Han, Y., Zalhaf, A.S., Lehtonen, M., Darwish, M.M., Mahmoud, K., 2024. Risk-averse bi-level planning model for maximizing renewable energy hosting capacity via empowering seasonal hydrogen storage. Appl. Energy 361, 122853. https://doi.org/10.1016/j.apenergy.2024.122853.

Zimmerman, R.D., Murillo-Sánchez, C.E., Thomas, R.J., 2009. MATPOWER's extensible optimal power flow architecture. In: 2009 IEEE Power & Energy Society General Meeting. IEEE, pp. 1–7.

Zimmerman, R.D., Murillo-Sánchez, C.E., Thomas, R.J., 2010. MATPOWER: Steady-state operations, planning, and analysis tools for power systems research and education. IEEE Trans. Power Syst. 26 (1), 12–19.

Zio, E., Aven, T., 2011. Uncertainties in smart grids behavior and modeling: What are the risks and vulnerabilities? How to analyze them? Energy Policy 39 (10), 6308–6320.